Journal of Photochemistry & Photobiology, A: Chemistry 434 (2023) 114278

Contents lists available at ScienceDirect

Journal of Photochemistry & Photobiology, A: Chemistry

journal homepage: www.elsevier.com/locate/jphotochem

Synthesis and characterization of a novel colorimetric and fluorometric probe "Turn-on" for the detection of Cu^{2+} of derivatives rhodamine

Camilo Segura [a], Osvaldo Yañez [b,c], Antonio Galdámez [d], Victoria Tapia [e], Marco T. Núñez [e], Igor Osorio-Román [a], Camilo García [f,*], Olimpo García-Beltrán [g,h,*]

[a] Instituto de Ciencias Químicas, Facultad de Ciencias, Universidad Austral de Chile, Valdivia 509000, Chile
[b] Facultad de Ingeniería y Negocios, Universidad de las Américas, Santiago, Chile
[c] Center of New Drugs for Hypertension (CENDHY), Santiago, Chile
[d] Department of Chemistry, Faculty of Science, University of Chile, Santiago, Chile
[e] Department of Biology, Faculty of Science, University of Chile, Santiago, Chile
[f] Universidad Católica de Temuco, Facultad de Recursos Naturales, Departamento de Ciencias Biológicas y Químicas, Avenida Rudecindo Ortega 02950, Campus San Juan Pablo II, Temuco, Chile
[g] Universidad Bernardo O'Higgins, Centro Integrativo de Biología y Química Aplicada (CIBQA), General Gana 1702, Santiago 8370854, Chile
[h] Facultad de Ciencias Naturales y Matemáticas, Universidad de Ibagué, Carrera 22 calle 67, Ibagué 730002, Colombia

ARTICLE INFO

Keywords:
Chemosensor
Colorimetric fluorescent dye
Cu^{2+} ions
Rhodamine derivate
Turn-On

ABSTRACT

A new Rhodamine-based "Turn On" fluorescent probe (E)- 3′,6′-bis(diethylamino)-2-((2,5-dimethoxybenzylidene)amino)spiro[isoindoline-1,9′-xanthen]-3-one (**WGB**) was synthesized. Results show that **WGB** is selective for Cu^{2+} cations, forming a **WGB**-Cu^{2+} complex in a 2:1 stoichiometry, confirmed through density functional theory (DFT) electronic structure calculations and reactive molecular dynamics (MD) simulations. Theoretical calculations agreed with the experimental data. The detection limit of **WGB**-Cu^{+2} complex is 6.76×10^{-8} M. Preliminary studies employing epifluorescence microscopy demonstrate that Cu^{2+} can be imaged in neuroblastoma SH-SY5Y cells treated with **WGB**.

1. Introduction

New fluorescence probe for the detection of Cu^{2+} ions have been developed in the last decade [1–4] and a wide range of fluorophores such as coumarin [5], bis(difluoroboron)-1,2-bis[(1H-pyrrol-2-yl) methylene] hydrazine (BOPHY) [6], p-dimethylaminobenzamide [7], rodhamine [8], curcumin [9], pyridoxal-5-phosphate [10] among others have been used and exploited in diverse applications [11–13]. Most fluorescent probes reported in the literature give a fluorescence quenching due to paramagnetic characteristics of this metal [14–17], thus there are few reports where they describe new fluorescent probes with an increase in the fluorescent response.

From the biological point of view copper is the third most abundant trace element in many living organisms including humans, serving as a catalytic co-factor for several metalloenzymes including bone formation [18], cellular respiration [19] and connective tissue development [20]. Studies have reported and demonstrated that this metal, when found in high concentrations exceeding normal may generate pathologies gastrointestinal disorders [21], dyslexia [22], and liver or kidney damage [23], Menkes syndrome [24], hypoglycemia, Prion disease [25], Alzheimer's disease [26], also a significant environment pollutant [27] and besides catalyzing the formation of reactive oxygen species (ROS) [28] that are capable of damaging biomolecules and involved in Parkinson's disease. Usually, to detect and quantify this ion there are different methods such as atomic absorption spectrometry [29], plasma atomic emission spectrometry [30], mass spectrometry [31], voltammetry [32], kinetic analysis [33], among others [34–36]. However, these traditional methods require expensive equipment. Among the techniques that stand out for their high sensitivity and that do not require sophisticated equipment is fluorescence, which allows the development of new sensors as an alternative method for the selective determination of analytes.

In this work, we present a novel colorimetric and fluorometric rhodamine derivative probe named **WGB**, which can selectively detect Cu^{2+} ions in aqueous solutions. In addition, **WGB** can be used in the environmental sciences to determine the presence of cupric ions in water

* Corresponding authors at: Facultad de Ciencias Naturales y Matemáticas, Universidad de Ibagué, Carrera 22 calle 67, Ibagué 730002, Colombia.
E-mail address: jose.garcia@unibague.edu.co (O. García-Beltrán).

https://doi.org/10.1016/j.jphotochem.2022.114278
Received 30 June 2022; Received in revised form 7 September 2022; Accepted 11 September 2022
Available online 15 September 2022

sources, due to its ability to discriminate qualitatively by colour change the presence of Cu^{2+} and in biological sciences as a fluorescent tool to determine the presence of Cu^{2+} in living cells. The theoretical computations were also done for the optimized geometric features of **WGB**-Cu^{2+} complex in a 2:1 and 1:1 stoichiometry. In addition, Reaxff reactive molecular dynamics simulations showed very stable 2:1 and 1:1 complex structure Cu^{2+} coordinated with **WGB** throughout of simulation.

2. Experimental

2.1. Materials and instruments

The reagents were purchased from Sigma-Aldrich and were used as received. Unless indicated otherwise, all solutions employed in this study were prepared in HEPES buffer (20 mM; pH 7.4). ^{1}H- and ^{13}C NMR spectra were recorded with a Bruker multidimensional 200 MHz spectrometer, using the solvent or the TMS signal as an internal standard. All chemical shifts are reported in the standard δ notation of parts per million. Absorption spectra were recorded at 25 °C using a Perkin Elmer model Lambda 11 spectrometer. Fluorescence spectra were obtained on an Edinburgh Instruments FLS900 fluorescence spectrometer. Data were recorded online and analyzed by Origin 8.0 software on a PC. All absorption and emission spectra were measured in a mixture of ACN: aqueous 20 mM HEPES buffer, pH 7.4, 1:1. The X-ray diffraction data were collected using a Bruker SMART platform CCD diffractometer with graphite-monochromatized Mo K⟨ radiation. The emission spectra were recorded on an ISS PC1 fluorescence spectrometer. The fluorescence imaging was measured using a Zeiss Hal 100 epifluorescence inverted microscope.

2.2. General synthetic conditions of (E)-3′,6′-bis(diethylamino)-2-((2,5-dimethoxybenzylidene)amino)spiro[isoindoline-1,9′-xanthen]-3-one (*WGB*)

A modification of the procedure [37] for the synthesis of II was employed. II was synthesized by a one-step reaction of rhodamine B (I) with hydrazine hydrate in methanol (Scheme1). To a 0.4 g of rhodamine B (I) dissolved in 15 ml of methanol, an excessive hydrazine hydrate (0.5 ml) was added and then the reaction solution was refluxed till the pink colour disappeared. After that, the cooled reaction solution was poured into distilled water and extracted with ethyl acetate (6 × 25 ml). The combined extracts were dried with sodium sulphate anhydrous, filtered, and then evaporated. Followed to 20 ml anhydrous ethanol was added II (0.23 g, 0.5 mmol), an excessive 2,5-dimethoxybenzaldehide (0.6 mmol) was added and the mixture was vigorously at room temperature for 24 h. The reaction progress was monitored by thin-layer chromatography. After completion of the reaction, the formed precipitate was filtered, washed with cold methanol (3 X 10 ml) and then dried in a vacuum, affording 0.17 g product. Obtained the compound **WGB**. ^{1}H NMR (*CDCl$_3$*): δ 9.0 (s, 1H, N = CH), 7.90 (d, 1H, ArH, J = 8.0 Hz), 7.58 (m, 2H, ArH), 7.11 (d, 2H, ArH, J = 8.0 Hz), 7.06 (d, 1H, ArH, J = 2.0 Hz), 6.89 (s, 1H, ArH), 6.49 (m, 6H, ArH), 3.66 (s, 3H, $-OCH_3$), 3.65 (s, 3H, $-OCH_3$), 3.30 (q, 8H, NCH_2CH_3), 1.07 (t, 12H, NCH_2CH_3). ^{13}C NMR (*CDCl$_3$*): δ 163.3, 153.0, 152.7, 152.5, 152.0, 148.2, 141.9, 133.5, 128.9, 128.5, 127.4, 127.2, 123.6, 123.3, 122.7, 117.2, 113.4, 108.3, 106.2, 96.8, 65.2, 55.9, 54.8, 43.4, 11.9. HRMS: $[M + Na]^+$, $C_{37}H_{40}N_4NaO_4$, found: 627.5370; calcd.: 627,2947.

2.3. Association constant (Benesi-Hildebrand Plot).

Fluorescence intensity data for the **WGB**-Cu^{2+} complex was plotted according to the Benesi-Hildebrand equation [38,39]:

$$1/(F - F_0) = 1/\{K_a{}^* \ (Fmax - F_0) \ * \ [Cu2+]\} + 1/(Fmax - F_0) \quad (1)$$

where Ka is the stability constant for 1:1 complex formation, F_0 is the total fluorescence intensity of the sensor (with 540 nm excitation) in the absence of Cu^{2+}, F is the observed total fluorescence intensity as a function of the Cu^{2+} concentration, and Fmax is the maximal total fluorescence intensity in the presence of Cu^{2+} in solution.

2.4. Calculation of the fluorescence quantum yield.

The fluorescence quantum yield was determined using quinine sulfate dissolved in 0.5 M H_2SO_4 (Φr = 0.546) as standard and was calculated using equation (2).[40].

$$\Phi s = \Phi r \ (ArFs/AsFr)(\eta s2/\eta r2) \quad (2)$$

where the subscripts s and r denote sample and reference, respectively; A is absorbance at the excitation wavelength (very dilute solutions), F is the integrated fluorescence intensity, and η is the refractive index of the medium.

2.5. Calculation of detection limit (LOD) and quantification limit (QOD)

LOD and QOD were determined using equation (3) and equation (4). [41].

$$LOD = (3S\_bl)/m \quad (3)$$

$$QOD = (10S\_bl)/m \quad (4)$$

Where Sbl is the standard deviation of the blank fluorescence measurement and m is the slope of the calibration curve. To determine the standard deviation of the blank, 10 fluorescence measurements of a 200 μM **WGB** solution were performed.

2.6. Computational methods

Quantum chemical calculation: The geometry optimization of the closed **WGB**, open **WGB**·Cu^{2+} and complex structure Cu^{2+} coordinated with **WGB** dimer was carried out with the density functional theory method by a hydrid functional B3LYP14 functional (Becke's Three Parameter Hybrid Functional Using the LYP Correlation Functional)

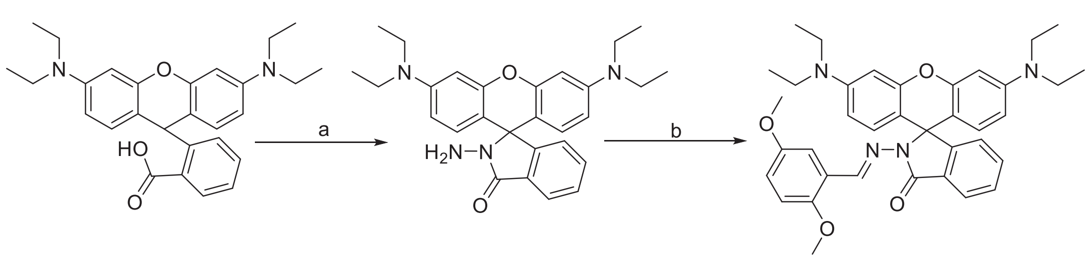

I II WGB

Scheme 1. Synthetic route to **WGB**. Reagents and conditions: a) hydrazine hydrate, MeOH, reflux; b) 2,4-dimethoxybenzaldehyde, r.t. 24 h.

with 6-31G(d,p) basis set. The quantum mechanics calculations were performed using the Gaussian 09 software [42].

Molecular Dynamics: The molecular dynamics (MD) simulations were performed using reactive force field [43] (ReaxFF). ReaxFF is a general bond-order-dependent force field method fitted to potentials derived from first principles DFT calculations, allowing chemical reactions to take place via the cleavage or formation of covalent chemical bonds during a MD run. The simulations were carried out using an explicit solvent with. Starting configurations were generated in cubic boxes with lateral dimensions of 26 Å. The systems were prepared by optimized closed **WGB**, open **WGB**·Cu^{2+} and complex structure Cu^{2+} coordinated with **WGB** dimer, and randomly placing water molecules in the simulation box using a packing molecule in defined regions of space called Packmol [44]. The ReaxFF parameters used in our simulation were adopted [45,46]. The simulations was performed under constant particle number, constant volume, and constant temperature (NVT ensemble with Berendsen thermostat) conditions for 1 ns, where we maintained target temperatures of 300 K and 1 atm. A relatively short time integration interval of $\Delta t = 0.1$ fs was chosen in the velocity Verlet algorithm. The simulations were performed using the LAMMPS platform [47,48].

2.7. Cell culture and fluorescence imaging.

Human neuroblastoma SH-SY5Y cells (CRL-2266, American Type Culture Collection, Rockville, MD) were cultured in MEM-F12 medium supplemented with 10 % fetal bovine serum (FBS), non-essential amino acids, antibiotic–antimycotic mixture, and 20 mM HEPES buffer, pH 7.2. The medium was replaced every 2 days. Cells were washed and the basal fluorescence was measured. They were then treated with **WGB** (5 µM, 20 min) and washed with FBS, after which their fluorescence was determined. The cells were then incubated with Cu-His (200 µM, 15 min) and their fluorescence determined again. The fluorescence was measured using a microplate fluorescence reader and by *epi*-fluorescence microscopy at 63 × amplification [49].

3. Results and discussion

The compound (*E*)-3′,6′-bis(diethylamino)-2-((2,5-dimethoxybenzylidene)amino)spiro[isoindoline-1,9′-xanthen]-3-one (**WGB**) was synthetized for modification of the procedure of Dujols et al.[37]. This compound was synthesized by a two-step reaction of rhodamine B (I) with hydrazine hydrate in methanol. The reaction solution was refluxed till the pink colour disappeared (II). An excessive 2,5-dimethoxybenzaldehide was added and the mixture was vigorously at room temperature for 24 h. The reaction progress was monitored and after completion of the reaction, the formed precipitate was filtered (Scheme 1), which was characterized by ^{1}H NMR and ^{13}C NMR spectroscopy (SI Fig. S1A and S1B), ESIMS (SI Fig. S1C) and crystallography data.

The skeleton of the molecule is shown in Fig. 1 and a summary of crystallographic data for the compound is given in Table S1 (SI Figs. S2 and S3). The xanthene and spirolactam in **WGB** rings are almost perpendicular to each other with a dihedral angle of 94.0°. The 5-membered ring (N1/C4/C16/C20/C14) adopts an envelope conformation on N1 atoms as indicated by the Cremer and Pople puckering parameters: Q2 is 0.089(2) Å and φ is 355.3(15)°. N1-N2 bond distance [1.376(2) Å] agrees well with the similar bonds in related compounds [50,51]. The torsion angle N1-N2-C13-C12, in **WGB**, is −172.92(17)°. All other relevant structural parameters (bond distances and angles) are as expected and in acceptable agreement with the described analogue [51–53] In the crystal packing of **WGB**, molecules are linked by C—H•••π and C—H•••O interactions (Fig. S3 and Table S2). The intermolecular interactions C—H•••π are above or below the plane of Cg centroids. The molecule contains an additional intramolecular C13-H13•••O2 contact (Fig. 1: bottom).

4. UV–Visible and fluorescence titrations on metal ions

In order to investigate the selectivity of **WGB** to different ions, UV–Visible and fluorescence spectroscopy studies were performed. Absorption spectrum of **WGB** shows four bands with maximums at 240, 278, 316 and 360 nm (Fig. 2B). The fluorescence spectrum of **WGB** is shown in Fig. S4B which has three maximums at 391, 414 and 536 nm. Upon 330 nm excitation, the emission quantum yield (ϕ) of **WGB** was determined to be $\phi = 0.00971$, using quinine sulphate as standard (SI Fig. S4A y S4B). To study the affinity of **WGB** to different ions, solutions of 20 µM **WGB** and 200 µM metal cations were prepared (Hg^{2+}, Fe^{2+}, Fe^{3+}, Ca^{2+}, Cd^{2+}, Co^{2+}, Cu^{2+}, Zn^{2+}, Mn^{2+}, Mg^{2+} and Pb^{2+}) in 20 mM HEPES buffer (pH 7.4). When Cu^{2+} ions were added, a colorimetric change was immediately observed (Fig. 2A), changes not observed with other study ions. Subsequently, the change in the UV–Visible spectrum of **WGB** in the presence of different ions was measured (Fig. 2B), showing the appearance of a new band with an absorption maximum located at 560 nm when incorporating Cu^{2+} ions (200 M) to a 20 M solution of **WGB**, confirming that there is a **WGB**-Cu^{2+} interaction type, while with the other cations there is no significant change in the UV–Visible spectrum of **WGA**, indicating its selectivity towards this cation. Since UV–Visible methods have low sensitivity, the change in fluorescence emission of **WGB** was studied. Fig. 2C shows that there is an approximately 7-fold increase in the emission intensity of **WGB** when Cu^{2+} cation is present in the solution. In contrast, the other cations do not show an enhancement in fluorescence emission, or it is of less

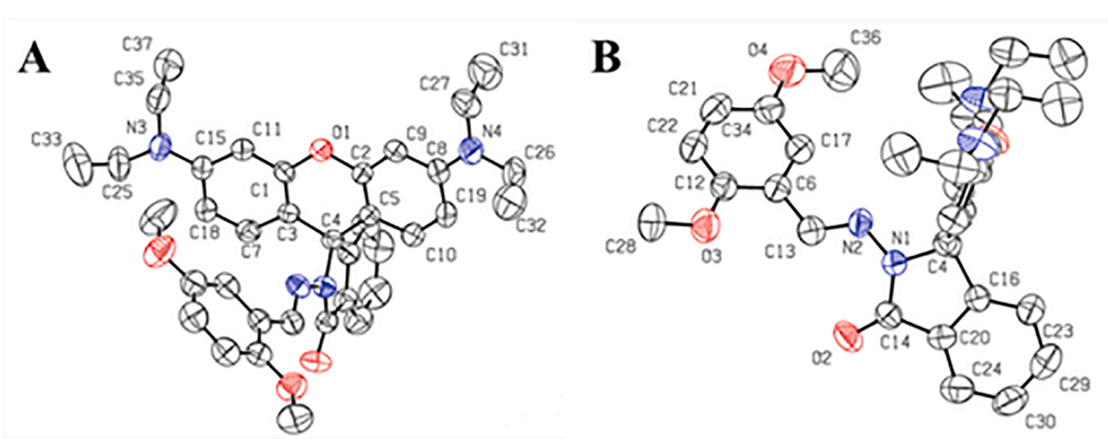

Fig. 1. Mutually approximately perpendicular views of the structure of (**WGB**) showing the atom numbering scheme (top, bottom). Displacement ellipsoids are drawn at the 50% probability level.

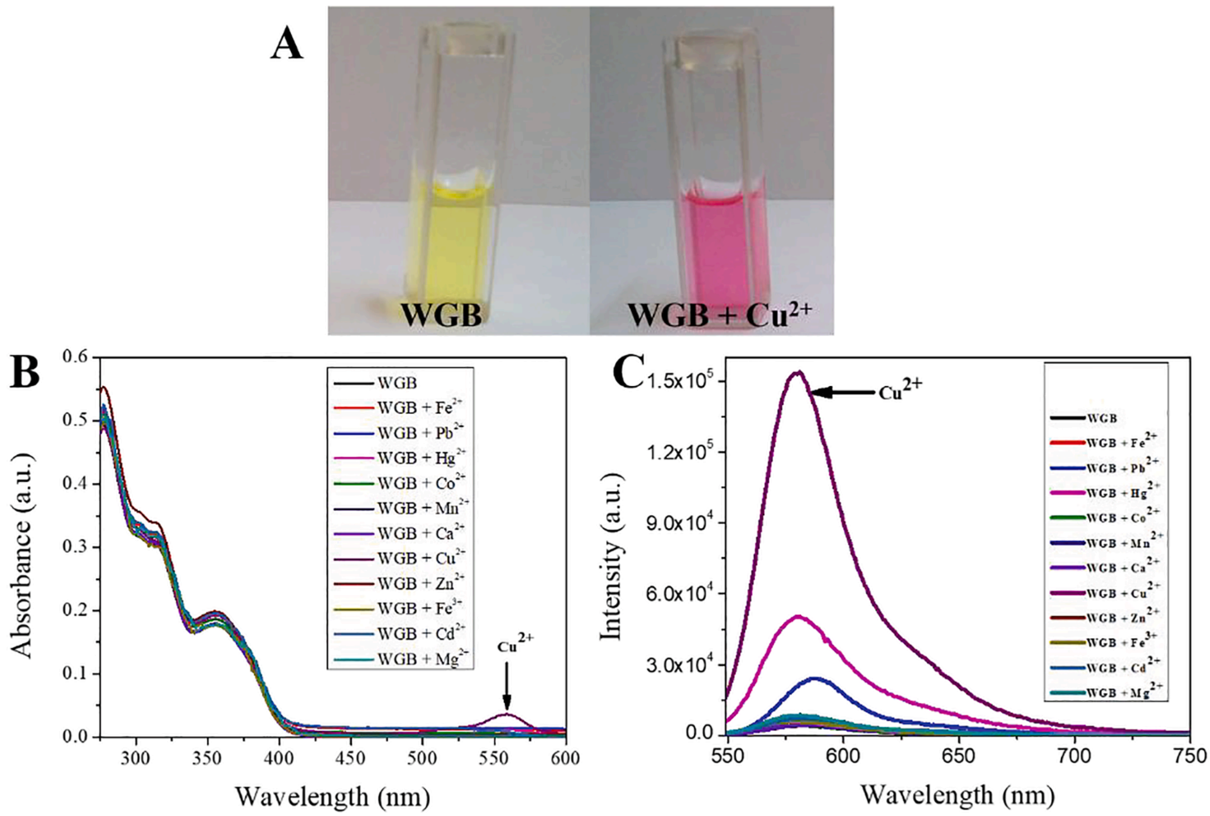

Fig. 2. A) colorimetric change of **WGB** in the presence of Cu^{2+} ion; B) UV–Visible C) Fluorescence spectra of **WGB** (20 μM) alone and in the presence of several different metal salts (Hg^{2+}, Fe^{2+}, Fe^{3+}, Ca^{2+}, Cd^{2+}, Co^{2+}, Cu^{2+}, Zn^{2+}, Mn^{2+}, Mg^{2+} and Pb^{2+}) in 20 mM HEPES buffer, pH 7.4.

intensity. These results indicate that the synthesized **WGB** molecule is selective for Cu^{2+} cation, forming a ́Turn On“ fluorescence metal ligand complex probe, this phenomenon is associated with the ring opening of the rhodamine spirolactam which in turn undergoes a charge transfer to one of the rhodamine ethylamino [54–56]. In addition, when performing interferent assays, it was determined that no changes were observed by the addition of other metals together with Cu^{2+} ions, which allows us to demonstrate and conclude that **WGB** is very selective for Cu^{+2} ions (Fig. 3). Additionally, reversibility was observed with EDTA, resulting in a decay in the 560 UV–vis band upon addition of an excess of this chelator and reestablished upon further addition of Cu^{2+} ions.

5. Fluorescence titrations on Cu^{2+} cation and stoichiometry

Fig. S5A shows the Cu^{2+} concentration-dependent emission fluorescence spectra of **WGB** (20 μM). When excited at 540 nm, the emission fluorescence intensity at 580 nm increases until reaching a value of 15-fold when the concentration of Cu^{2+} increases from 0 to 200 μM. From this data a calibration curve was performed to determine the detection and quantification limit of Cu^{2+} through the formation of the fluorescent complex **WGB**-Cu^{2+}. A linear relationship between Cu^{2+} concentration and total fluorescence intensity was performed. The linear fit gives the equation $Y = 0.0073 * x + 0.91$. With these data, the limit of detection and quantification are calculated to be 6.76×10^{-8} M and 2.25×10^{-7} M respectively (SI Fig. S5B). These values are in the concentration.

range of other similar probes [57] used for the determination of Cu^{2+} and show that **WGB** can be used for the determination of Cu^{2+} in environmental and biological samples. Table 1 shows a comparison between different copper sensors and the one synthesized in this work.

On the other hand, a Benesi–Hildebrand [38] graph of the fluorescence was made from data in Fig. S5A (SI Fig. S6) which was non-linear, indicating that the stoichiometry of the Cu^{2+} complex formed is

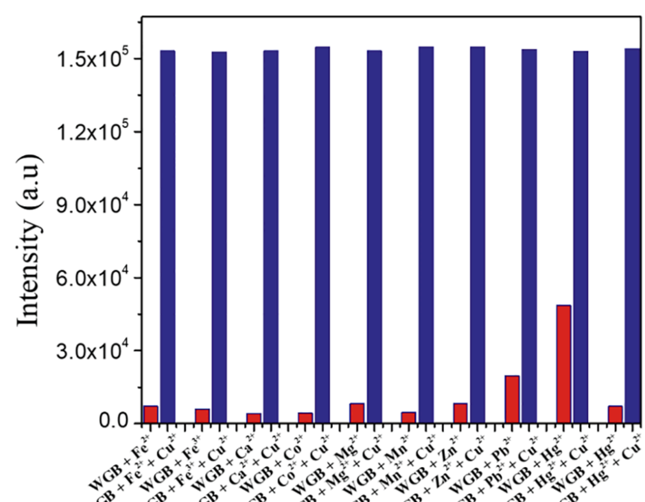

Fig. 3. Selectivity of the fluorescence enhancement for **WGB** (20 μM) alone and in the presence of several different metal salts (Hg2+, Fe2+, Fe3+, Ca2+, Cd2+, Co2+, Cu2+, Zn2+, Mn2+, Mg2 + and Pb2 +) in 20 mM HEPES buffer, pH 7.4. Red bars indicate the fluorometric responses of **WGB** with 10 equivalents of Fe^{+2}, Fe^{+3}, Ca^{+2}, Co^{+2}, Mg^{+2}, Mn^{+2}, Zn^{+2}, Cd^{+2}, Pb^{+2}, and Hg^{+2} and blue bars represent the fluorescence response after the addition of the same ions and 10 equivalent of Cu^{+2}. (For interpretation of the references to colour in this figure legend, the reader is referred to the web version of this article.)

different from 1:1. Consistent with this, application of the Method of Continuous Variation resulted in a Job's plot (SI Fig. S5C) with a maximum at a mole fraction of Cu^{2+} close to 0.33, indicating a preferred 2:1 stoichiometry for the complex. To corroborate these results, the

Table 1
Comparison of some colorimetric and fluorometric sensors for Cu^{2+} detection.

Chemosensor	Signal process	Solvent media	Detection limit	Reference
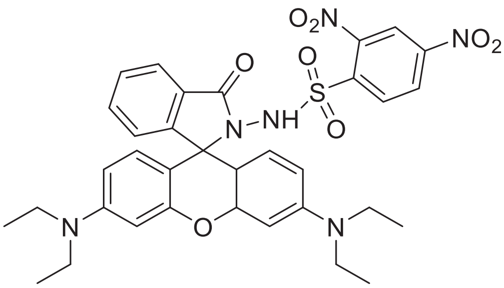	Fluorescence Turn-On	$CH_3CN:H_2O$ (1:1; v/v)	4.7 X 10^{-9} M	[58]
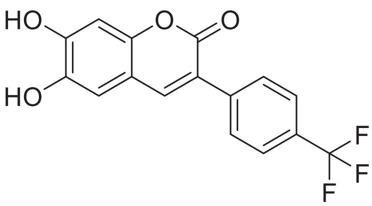	Fluorescence Turn-Off	CH_3CN:HEPES (95:5; v/v)	2.45 X 10^{-8} M	[59]
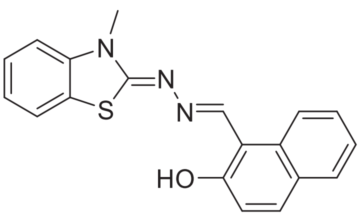	Fluorescence Turn-On	CH_3CN	3.3 X 10^{-6} M	[60]
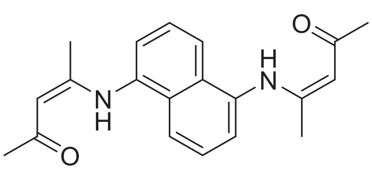	Fluorescence Turn-Off	H_2O:DMF (9:1 v/v)	1.0 X 10^{-7} M	[61]
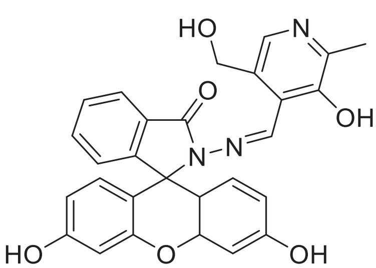	Colorimetric	CH_3OH:HEPES (1:1; v/v)	1.5 X 10^{-6} M	[62]
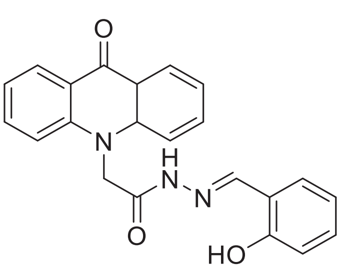	Fluorescence Turn-Off, Colorimetric	DMSO:H_2O (4:1; v/v)	8.0 X 10^{-5} M	[63]
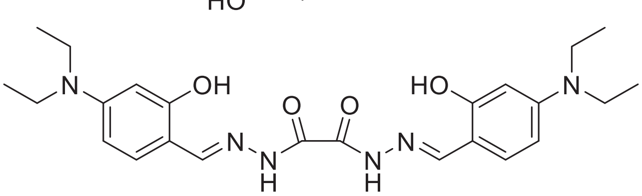	Fluorescence Turn-Off, Colorimetric	DMSO:H_2O (7:3, v/v)	1.2 X 10^{-7} M	[64]

(continued on next page)

Table 1 (*continued*)

Chemosensor	Signal process	Solvent media	Detection limit	Reference
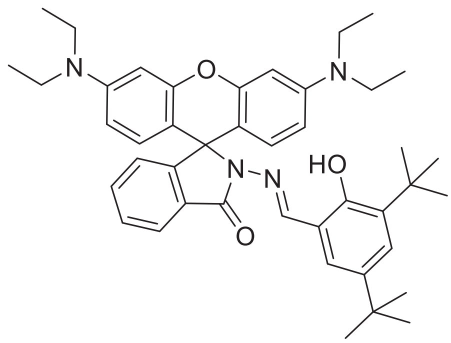	Fluorescence Turn-On, Colorimetric	EtOH:HEPES (1:1, v/v)	1.16 X 10^{-6} M	[65]
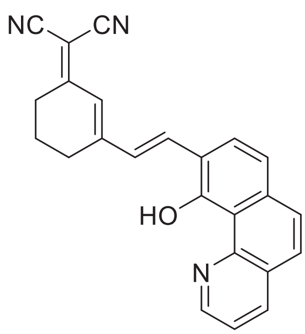	Colorimetric	$CH_3CN:H_2O$ (7:3, v/v)	1.41 × 10^{-7} M	[66]
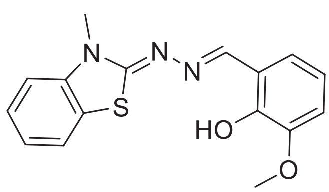	Colorimetric	CH_3CN	3.7 × 10^{-7} M	[67]
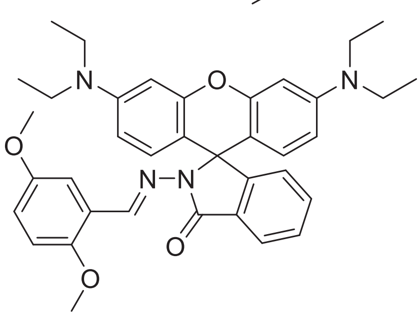	Fluorescence Turn-On, Colorimetric	20 mM HEPES in water	6.76 × 10^{-8} M	This work

logarithms of the formation constants of the **WGB**-Cu^{2+} complexes with stoichiometries 1:1 and 2:1 (log K1 and log K2) were calculated using the maximum probability software KEV [68,69] (adjusted $R^2 = 0.986$). For the **WGB**-Cu^{2+} 1:1 log K1 complex it is equal to 4.00 while for the **WGB**-Cu 2:1 log K2 complex it is equal to 7.86. This indicates that the **WGB**-Cu^{2+} 2:1 complex is the one that forms mainly as indicated by the Jobs diagram.

6. Computational analysis

Reactive molecular dynamics using Reaxff simulations showed a very stable complex structure Cu^{2+} coordinated with **WGB** throughout the 1 ns of simulation, see Fig. 4. The average angle (∠ O1—N2—O2) of closed **WGB** and open complex **WGB**·Cu^{2+}, is 105° and 111°. These angles indicate that the **WGB** opens to capture and establish copper-centred coordination. In addition, the simulations showed very stable potential energy throughout the 1.0 ns of simulation.

The evaluation of the DFT calculations showed a very stable complex structure Cu^{2+} coordinated with **WGB** (Fig. 4), indicating that coordination of copper and complexes of **WGB** have *trans*-bidentate no square-planar geometry. The average bond lengths between N1,2—Cu^{2+} and O1,2—Cu^{2+} are 2.290 Å and 1.846 Å. These distances indicate that copper binds to N and O. The Copper-centered coordination average angles for N1,2—Cu^{2+}—O1,2, N1—Cu^{2+}—N2 and O1—Cu^{2+}—O2 are 91.492°, 27.840° and 172.681°. The bond length (C4—N1) of closed **WGB** and open complex **WGB**-Cu^{2+}, is 1.504 Å and 2.846 Å.

These bond lengths indicate the **WGB** opens to capture and establish copper-centred coordination. Moreover, the stoichiometry of association ligand–metal **WGB**-Cu^{2+} was determined based on Job's method (SI. Fig. S5C). The results exhibited that the fluorescence went through a maximum when the molecular fraction was close to 0.32, which indicated 2:1 stoichiometry. The electron distributions (Fig. 5a-l) of HOMO, LUMO and LUMO + 2 of open **WGB**-Cu^{2+} and complex structure Cu^{2+} coordinated with **WGB** dimer. The electronic distribution on LUMO + 2 for the complex was extended to Cu^{2+}, indicating the electron transfer from HOMO to LUMO + 2.

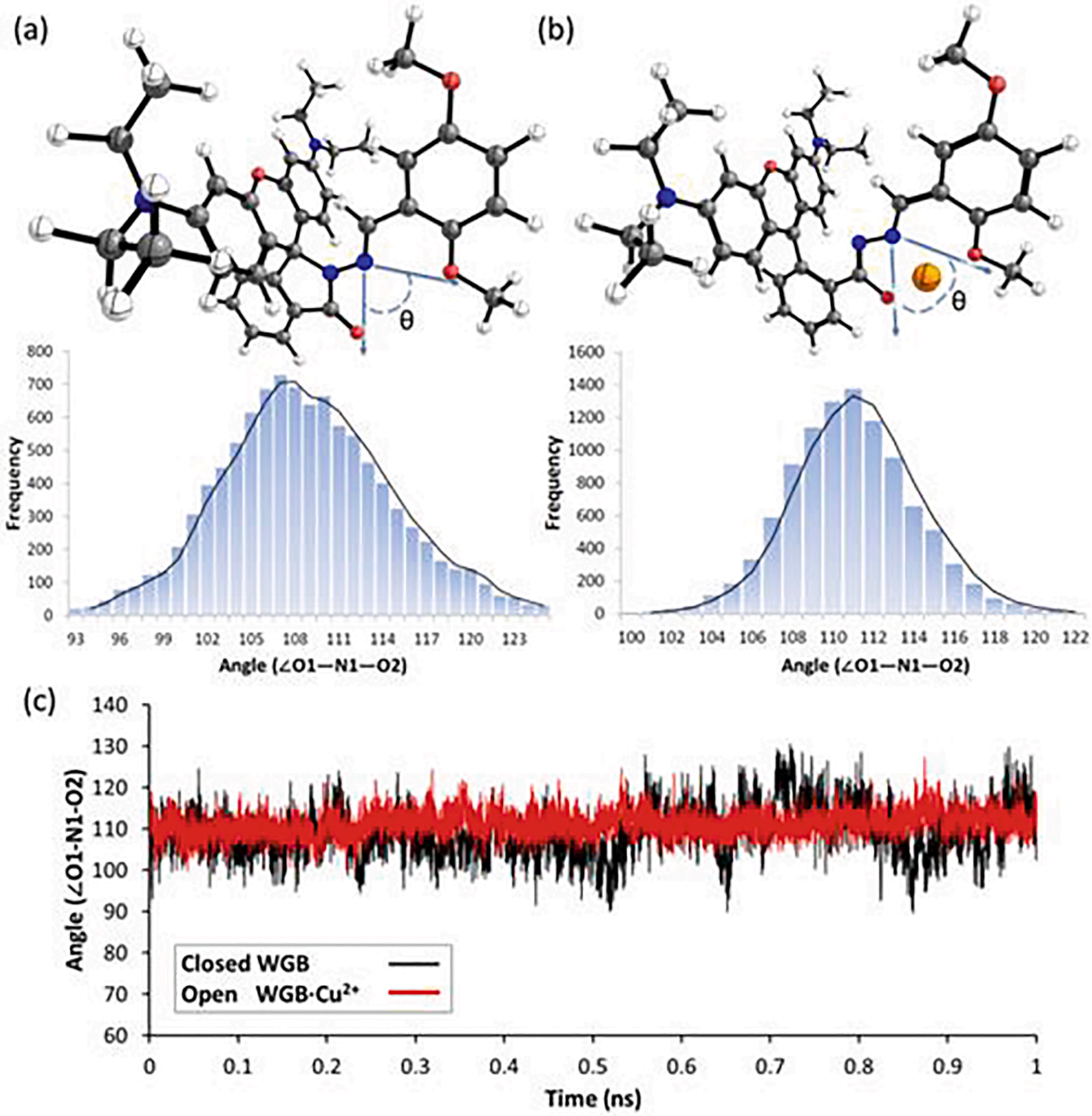

Fig. 4. Angles (O1—N1—O2) of closed **WGB** (a) and open **WGB**·Cu^{2+} (b) as frequency distribution and (c) function of time.

7. In vitro test

There are several reports in the literature on the development of fluorescent probes for copper, however, those showing a "Turn On" mechanism is scarce. **WGB** is a compound synthesised from rhodamine, this compound is characterised by the presence of diethylamino groups that show affinity for cell membranes and a spirolactam, this last characteristic allows that when chelating **WGB**-Cu^{2+} the ring opens and a "Turn On" mechanism is observed. When performing the cellular assays to determine if there was any preference of this probe for any type of cellular structure, initially neuroblastoma cell lines (SH-SY5Y) were incubated and microscopic observation was performed, observing a null fluorescence. Subsequently, **WGB** was added in physiological conditions and incubated with SH-SY5Y cells (Fig. 6A), observing the same behaviour, then the cells were treated with the histidine-Cu^{+2} complex as a source of Cu^{2+}. Fluorescence was monitored by epifluorescence microscopy. A significant increase in fluorescence was observed (Fig. 6B) after addition of histidine-Cu^{+2}, showing a distribution in the cell body.

8. Conclusions

In this study we report the synthesis and structural characterisation of a rhodamine-derived compound called **WGB**, which was tested for selectivity and sensitivity to ions of biological interest and environmental (Fe^{2+}, Fe^{3+}, Ca^{2+}, Co^{2+}, Cu^{2+}, Mg^{2+}, Mn^{2+}, Zn^{2+}, Cd^{2+}, Pb^{2+}, and Hg^{2+}), showing that in the presence of Cu^{2+} ions colorimetric changes are observed and there is a substantial increase in fluorescence (Turn-on), probably associated with ring opening of the rhodamine spirolactam with charge transfer to one of the ethylamino of rhodamine. On the other hand, when interference tests were performed with the other ions under study, only slight changes were observed in the presence of Hg^{2+} and Pb^{2+} ions, showing a stable behaviour of the sensor. **WGB** shows a limit of detection and quantification estimated at 6.76×10^{-8} M and 2.25×10^{-7} M respectively. Furthermore, it showed a 2:1 ligand:metal association stoichiometry, which was confirmed through DFT and molecular dynamics calculations. Finally, **WGB** was evaluated as a molecular sensor in SH-SY5Y cells, and the fluorescence images obtained show that **WGB** has potential for biological application.

Associated Content.

(Word Style "TE_Supporting_Information"). Supporting

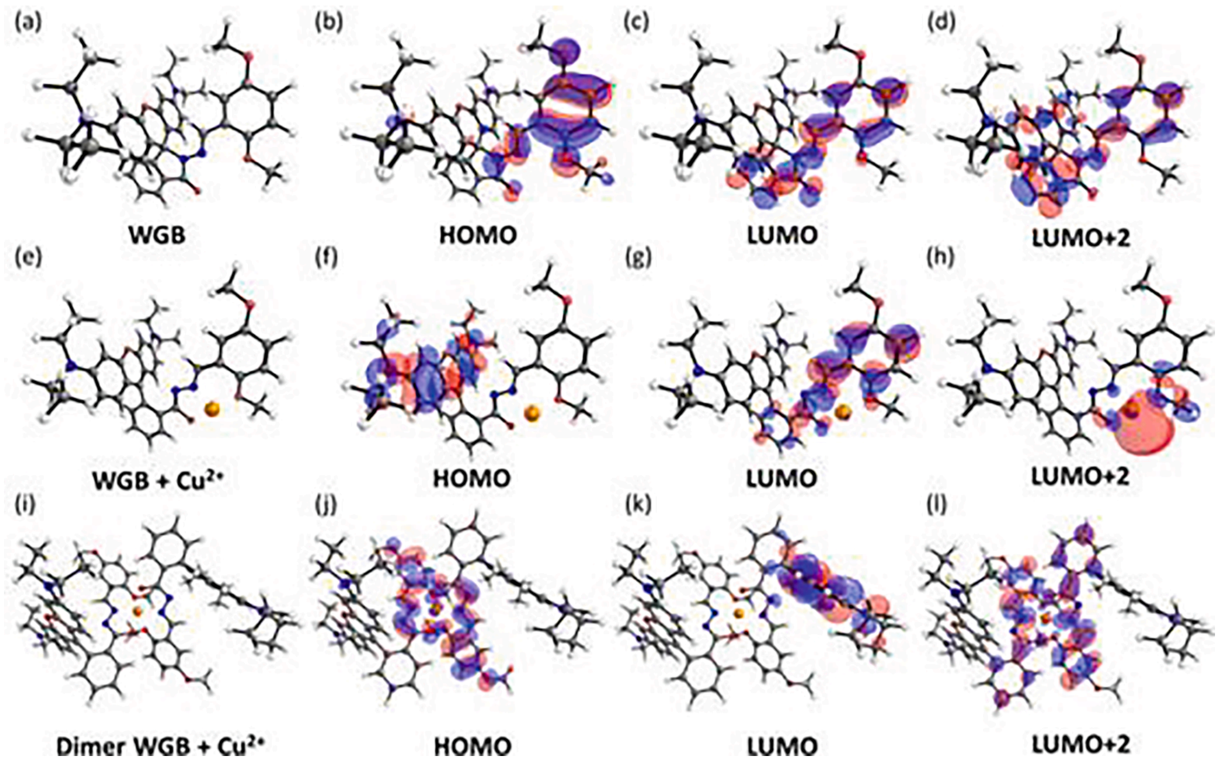

Fig. 5. The optimized geometry and calculated frontier molecular orbitals of the closed **WGB** (a-d), open **WGB**·Cu^{2+} (e-h) and complex structure Cu^{2+} coordinated with **WGB** dimer (i-l), obtained using B3LYP/6-31G(d,p) level. The plot was created with Chemcraft [70].

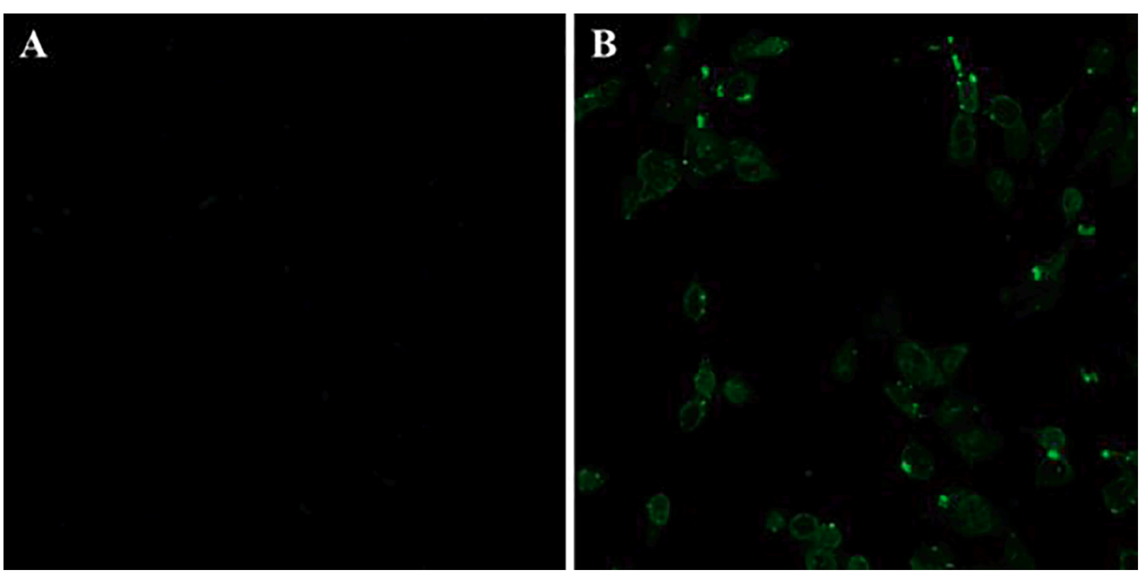

Fig. 6. In vitro tests of the potential of **WGB** as a cell probe for Cu^{2+}. (A) SH-SY5Y cells were incubated with **WGB** (5 μM, 20 min) and washed, and the basal fluorescence measured. (B) The cells were then incubated with Cu-His (200 μM, 25 min). The fluorescence was recorded by confocal microscopy, 63X objective.

Information. A listing of the contents of each file supplied as Supporting Information should be included. For instructions on what should be included in the Supporting Information as well as how to prepare this material for publications, refer to the journal's Instructions for Authors.

The following files are available free of charge.

brief description (file type, i.e., PDF)

brief description (file type, i.e., PDF)

Author Information

Author Contributions

O.G-B., C.G., C.S., and I.O-R., conceived and designed the experiments. A.G., X-ray crystallography study. O.Y., design and developed theoretical calculations. V.T. and M.T.N., Cellular assays.

CRediT authorship contribution statement

Camilo Segura: Methodology, Formal analysis. **Osvaldo Yañez:** Writing – original draft, Methodology, Formal analysis. **Antonio Galdámez:** Writing – original draft, Methodology, Formal analysis. **Victoria Tapia:** Methodology. **Marco T. Núñez:** Methodology, Conceptualization. **Igor Osorio-Román:** Writing – original draft, Validation, Methodology, Formal analysis. **Camilo Garcia:** Methodology, Formal analysis. **Olimpo García-Beltrán:** Writing – review & editing, Writing – original draft, Supervision, Project administration, Methodology, Investigation, Funding acquisition, Formal analysis, Conceptualization.

Declaration of Competing Interest

The authors declare that they have no known competing financial interests or personal relationships that could have appeared to influence the work reported in this paper.

Data availability

Data will be made available on request.

Acknowledgment

This work was supported by COLCIENCIAS Grant #130774559056 Colombia. The authors acknowledge to the projects ANID-FONDECYT #1190246 and FONDECYT Postdoctorado 2022 #3220178.

Appendix A. Supplementary data

Supplementary data to this article can be found online at https://doi.org/10.1016/j.jphotochem.2022.114278.

References

[1] Q. Zhang, R. Ma, Z. Li, Z. Liu, A multi-responsive crown ether-based colorimetric/fluorescent chemosensor for highly selective detection of Al3+, Cu2+ and Mg2+, Spectrochim. Acta - Part A Mol. Biomol. Spectrosc. 228 (2020) 117857. 10.1016/j.saa.2019.117857.

[2] D.J. Fanna, L.M.P. Lima, G. Wei, F. Li, J.K. Reynolds, A colorimetric chemosensor for quantification of exchangeable Cu2+ in soil, Chemosphere. 238 (2020), https://doi.org/10.1016/j.chemosphere.2019.124664.

[3] S. Li, D. Cao, X. Meng, Z. Hu, Z. Li, C. Yuan, T. Zhou, X. Han, W. Ma, A novel fluorescent chemosensor based on coumarin and quinolinyl-benzothiazole for sequential recognition of Cu2+ and PPi and its applicability in live cell imaging, Spectrochim. Acta - Part A Mol. Biomol. Spectrosc. 230 (2020) 118022. 10.1016/j.saa.2019.118022.

[4] W.W. Wang, Y. Wang, W.N. Wu, X.L. Zhao, Z.Q. Xu, Z.H. Xu, X.X. Li, Y.C. Fan, Pyrrole-quinazoline derivative as an easily accessible turn-off optical chemosensor for Cu2+ and resultant Cu2+ complex as a turn-on sensor for pyrophosphate in almost neat aqueous solution, Spectrochim. Acta - Part A Mol. Biomol. Spectrosc. 226 (2020) 117592. 10.1016/j.saa.2019.117592.

[5] M.H. Mahnashi, A.M. Mahmoud, S.A. Alkahtani, R. Ali, M.M. El-Wekil, A novel imidazole derived colorimetric and fluorometric chemosensor for bifunctional detection of copper (II) and sulphide ions in environmental water samples, Spectrochim. Acta - Part A Mol. Biomol. Spectrosc. 228 (2020) 117846. 10.1016/j.saa.2019.117846.

[6] Y. Li, H. Zhou, S. Yin, H. Jiang, N. Niu, H. Huang, S.A. Shahzad, C. Yu, A BOPHY probe for the fluorescence turn-on detection of Cu2+, Sensors Actuators, B Chem. 235 (2016) 33–38, https://doi.org/10.1016/j.snb.2016.05.055.

[7] P.C. Huang, H. Fang, J.J. Xiong, F.Y. Wu, Ultrasensitive turn-on fluorescence detection of Cu2 + based on p-dimethylaminobenzamide derivative and the application to cell imaging, Spectrochim. Acta - Part A Mol. Biomol. Spectrosc. 173 (2017) 264–269, https://doi.org/10.1016/j.saa.2016.09.011.

[8] K. Wechakorn, S. Prabpai, K. Suksen, P. Kanjanasirirat, Y. Pewkliang, S. Borwornpinyo, P. Kongsaeree, A rhodamine-triazole fluorescent chemodosimeter for Cu2+ detection and its application in bioimaging, Luminescence. 33 (2018) 64–70, https://doi.org/10.1002/bio.3373.

[9] G. Xu, J. Wang, G. Si, M. Wang, X. Xue, B. Wu, S. Zhou, A novel highly selective chemosensor based on curcumin for detection of Cu2+ and its application for bioimaging, Sensors Actuators, B Chem. 230 (2016) 684–689, https://doi.org/10.1016/j.snb.2016.02.110.

[10] D. Sharma, A. Kuba, R. Thomas, R. Kumar, H.J. Choi, S.K. Sahoo, An aqueous friendly chemosensor derived from vitamin B6 cofactor for colorimetric sensing of Cu2+ and fluorescent turn-off sensing of Fe3+, Spectrochim. Acta - Part A Mol, Biomol. Spectrosc. 153 (2016) 393–396, https://doi.org/10.1016/j.saa.2015.08.051.

[11] S. Cao, Q. Jin, L. Geng, L. Mu, S. Dong, A "turn-on" fluorescent probe for the detection of Cu2+ in living cells based on a signaling mechanism of NN isomerization, New J. Chem. 40 (2016) 6264–6269, https://doi.org/10.1039/c5nj03649f.

[12] W. Lin, L. Long, B. Chen, W. Tan, W. Gao, Fluorescence turn-on detection of Cu2+ in water samples and living cells based on the unprecedented copper-mediated dihydrorosamine oxidation reaction, Chem. Commun. 46 (2010) 1311–1313, https://doi.org/10.1039/b919531a.

[13] M. Kaur, M.J. Cho, D.H. Choi, A phenothiazine-based "naked-eye" fluorescent probe for the dual detection of Hg2+ and Cu2+: Application as a solid state sensor, Dye. Pigment. 125 (2016) 1–7, https://doi.org/10.1016/j.dyepig.2015.09.030.

[14] H.F. Xie, C.J. Yu, Y.L. Huang, H. Xu, Q.L. Zhang, X.H. Sun, X. Feng, C. Redshaw, A turn-off fluorescent probe for the detection of Cu2+ based on a tetraphenylethylene-functionalized salicylaldehyde Schiff-base, Mater. Chem. Front. 4 (2020) 1500–1506, https://doi.org/10.1039/c9qm00759h.

[15] P.N. Borase, P.B. Thale, G.S. Shankarling, Dihydroquinazolinone based "turn-off" fluorescence sensor for detection of Cu2+ ions, Dye. Pigment. 134 (2016) 276–284, https://doi.org/10.1016/j.dyepig.2016.07.025.

[16] R. Nagarajan, H.I. Ryoo, B.D. Vanjare, N. Gyu Choi, K. Hwan Lee, Novel phenylalanine derivative-based turn-off fluorescent chemosensor for selective Cu2 + detection in physiological pH, J. Photochem. Photobiol. A Chem. 418 (2021), 113435, https://doi.org/10.1016/j.jphotochem.2021.113435.

[17] A.K. Mahapatra, G. Hazra, N.K. Das, S. Goswami, A highly selective triphenylamine-based indolylmethane derivatives as colorimetric and turn-off fluorimetric sensor toward Cu2+ detection by deprotonation of secondary amines, Sensors Actuators, B Chem. 156 (2011) 456–462, https://doi.org/10.1016/j.snb.2011.04.009.

[18] C. Palacios, The role of nutrients in bone health, from A to Z, Crit. Rev. Food Sci. Nutr. 46 (2006) 621–628, https://doi.org/10.1080/10408390500466174.

[19] D. Strausak, J.F.B. Mercer, H.H. Dieter, W. Stremmel, G. Multhaup, Copper in disorders with neurological symptoms: Alzheimer's, Menkes, and Wilson diseases, Brain Res. Bull. 55 (2001) 175–185, https://doi.org/10.1016/S0361-9230(01)00454-3.

[20] V. Desai, S.G. Kaler, Role of copper in human neurological disorders, Am. J. Clin. Nutr. 88 (2008) 855–858, https://doi.org/10.1093/ajcn/88.3.855s.

[21] M. Araya, M. Olivares, F. Pizarro, M. González, H. Speisky, R. Uauy, Gastrointestinal symptoms and blood indicators of copper load in apparently healthy adults undergoing controlled copper exposure, Am. J. Clin. Nutr. 77 (2003) 646–650, https://doi.org/10.1093/ajcn/77.3.646.

[22] I.D. Capel, M.H. Pinnock, H.M. Dorrell, D.C. Williams, E.C. Grant, Comparison of concentrations of some trace, bulk, and toxic metals in the hair of normal and dyslexic children, Clin. Chem. 27 (1981) 879–881, https://doi.org/10.1093/clinchem/27.6.879.

[23] I. Bremner, Manifestations of copper excess, Am. J. Clin. Nutr. 67 (1998), https://doi.org/10.1093/ajcn/67.5.1069S.

[24] S.G. Kaler, Diagnosis and therapy of Menkes syndrome, a genetic form of copper deficiency, Am. J. Clin. Nutr. 67 (1998), https://doi.org/10.1093/ajcn/67.5.1029S.

[25] D.R. Brown, Copper and prion disease, Brain Res. Bull. 55 (2001) 165–173, https://doi.org/10.1016/S0361-9230(01)00453-1.

[26] Y.H. Hung, A.I. Bush, R.A. Cherny, Copper in the brain and Alzheimer's disease, J. Biol. Inorg. Chem. 15 (2010) 61–76, https://doi.org/10.1007/s00775-009-0600-y.

[27] P. Higueras, R. Oyarzun, J. Oyarzún, H. Maturana, J. Lillo, D. Morata, Environmental assessment of copper-gold-mercury mining in the Andacollo and Punitaqui districts, northern Chile, Appl. Geochemistry. 19 (2004) 1855–1864, https://doi.org/10.1016/j.apgeochem.2004.04.001.

[28] B. Halliwell, Reactive Oxygen Species and the Central Nervous System, J. Neurochem. 59 (1992) 1609–1623, https://doi.org/10.1111/j.1471-4159.1992.tb10990.x.

[29] Z. Es'haghi, R. Azmoodeh, Hollow fiber supported liquid membrane microextraction of Cu2+ followed by flame atomic absorption spectroscopy determination, Arab. J. Chem. 3 (1) (2010) 21–26.

[30] K. Sreenivasa Rao, T. Balaji, T. Prasada Rao, Y. Babu, G.R.K. Naidu, Determination of iron, cobalt, nickel, manganese, zinc, copper, cadmium and lead in human hair by inductively coupled plasma-atomic emission spectrometry, Spectrochim. Acta - Part B At. Spectrosc. 57 (2002) 1333–1338, https://doi.org/10.1016/S0584-8547(02)00045-9.

[31] M.S. Glover, J.M. Dilger, F. Zhu, D.E. Clemmer, The binding of Ca2+, Co2+, Ni2+, Cu 2+, and Zn2+ cations to angiotensin i determined by mass spectrometry based techniques, Int. J. Mass Spectrom. 354–355 (2013) 318–325, https://doi.org/10.1016/j.ijms.2013.06.014.

[32] M.A. Nolan, S.P. Kounaves, Microfabricated array of iridium microdisks as a substrate for direct determination of Cu2+ or Hg2+ using square-wave anodic stripping voltammetry, Anal. Chem. 71 (1999) 3567–3573, https://doi.org/10.1021/ac990126i.

[33] A.E. Murekhina, D.N. Yarullin, M.A. Sovina, P.A. Kitaev, G.A. Gamov, Copper (II) -Catalyzed Oxidation of Ascorbic Acid : Ionic Strength Effect and Analytical Use in Aqueous Solution, (2022) 1–12.

[34] Q. He, Z. Hu, Y. Jiang, X. Chang, Z. Tu, L. Zhang, Preconcentration of Cu(II), Fe(III) and Pb(II) with 2-((2-aminoethylamino)methyl)phenol-functionalized activated carbon followed by ICP-OES determination, J. Hazard. Mater. 175 (2010) 710–714, https://doi.org/10.1016/j.jhazmat.2009.10.067.

[35] M.A. Deshmukh, R. Celiesiute, A. Ramanaviciene, M.D. Shirsat, A. Ramanavicius, EDTA_PANI/SWCNTs nanocomposite modified electrode for electrochemical determination of copper (II), lead (II) and mercury (II) ions, Electrochim. Acta. 259 (2018) 930–938, https://doi.org/10.1016/j.electacta.2017.10.131.

[36] Y. Cao, J. Li, J. Liu, H. Liu, Y. Jiang, H. Zhang, Preparation and characterisation of a novel copper-imprinted polymer based on β-cyclodextrin copolymers for selective determination of Cu 2+ ions, Polym. Int. 68 (2019) 694–699, https://doi.org/10.1002/pi.5752.

[37] V. Dujols, F. Ford, A.W. Czarnik, A long-wavelength fluorescent chemodosimeter selective for Cu(II) ion in water, J. Am. Chem. Soc. 119 (1997) 7386–7387, https://doi.org/10.1021/ja971221g.
[38] H.A. Benesi, J.H. Hildebrand, A Spectrophotometric Investigation of the Interaction of Iodine with Aromatic Hydrocarbons, J. Am. Chem. Soc. 71 (1949) 2703–2707, https://doi.org/10.1021/ja01176a030.
[39] S.R. Liu, S.P. Wu, An NBD-based sensitive and selective fluorescent sensor for copper(II) ion, J. Fluoresc. 21 (2011) 1599–1605, https://doi.org/10.1007/s10895-011-0848-9.
[40] O. García-Beltrán, N. Mena, E.G. Pérez, B.K. Cassels, M.T. Nuñez, F. Werlinger, D. Zavala, M.E. Aliaga, P. Pavez, The development of a fluorescence turn-on sensor for cysteine, glutathione and other biothiols. A kinetic study, Tetrahedron Lett. (2011), https://doi.org/10.1016/j.tetlet.2011.09.137.
[41] M.E. Aliaga, M. Gazitua, A. Rojas-Bolaños, M. Fuentes-Estrada, D. Durango, O. García-Beltrán, A selective thioxothiazolidin-coumarin probe for Hg^{2+} based on its desulfurization reaction. Exploring its potential for live cell imaging, Spectrochim. Acta - Part A Mol. Biomol. Spectrosc. 224 (2020) 117372. 10.1016/j.saa.2019.117372.
[42] M.J. Frisch, G.W. Trucks, H.B. Schlegel, G.E. Scuseria, M.A. Robb, J.R. Cheeseman, G. Scalmani, V. Barone, B. Mennucci, G.A. Petersson, H. Nakatsuji, M. Caricato, X. Li, H.P. Hratchian, A.F. Izmaylov, J. Bloino, G. Zheng, J.L. Sonnenberg, M. Hada, M. Ehara, K. Toyota, R. Fukuda, J. Hasegawa, M. Ishida, T. Nakajima, Y. Honda, O. Kitao, H. Nakai, T. Vreven, J.A. Montgomery, J.E. Peralta, F. Ogliaro, M. Bearpark, J.J. Heyd, E. Brothers, K.N. Kudin, V.N. Staroverov, R. Kobayashi, J. Normand, K. Raghavachari, A. Rendell, J.C. Burant, S.S. Iyengar, J. Tomasi, M. Cossi, N. Rega, J. M. Millam, M. Klene, J.E. Knox, J.B. Cross, V. Bakken, C. Adamo, J. Jaramillo, R. Gomperts, R.E. Stratmann, O. Yazyev, A.J. Austin, R. Cammi, C. Pomelli, J.W. Ochterski, R.L. Martin, K. Morokuma, V.G. Zakrzewski, G.A. Voth, P. Salvador, J.J. Dannenberg, S. Dapprich, A.D. Daniels, Farkas, J.B. Foresman, J. V Ortiz, J. Cioslowski, D.J. Fox, Gaussian 09, Revision C.01, Gaussian 09, Revis. C.01, Gaussian, Inc., Wallingford CT. (2010).
[43] A.C.T. van Duin, S. Dasgupta, F. Lorant, W.A. Goddard, ReaxFF: A Reactive Force Field for Hydrocarbons, J. Phys. Chem. A. 105 (2001) 9396–9409, https://doi.org/10.1021/jp004368u.
[44] L. Martínez, R. Andrade, E.G. Birgin, J.M. Martínez, Packmol: A package for building initial configurations for molecular dynamics simulations, J. Comput. Chem. 30 (2009) 2157–2164, https://doi.org/10.1002/jcc.21224.
[45] O. Rahaman, A.C.T. van Duin, W.A. Goddard, D.J. Doren, Development of a ReaxFF Reactive Force Field for Glycine and Application to Solvent Effect and Tautomerization, J. Phys. Chem. B. 115 (2) (2011) 249–261.
[46] S. Monti, A. Corozzi, P. Fristrup, K.L. Joshi, Y.K. Shin, P. Oelschlaeger, A.C.T. Van Duin, V. Barone, Exploring the conformational and reactive dynamics of biomolecules in solution using an extended version of the glycine reactive force field, Phys. Chem. Chem. Phys. 15 (2013) 15062–15077, https://doi.org/10.1039/c3cp51931g.
[47] S. Plimpton, Fast Parallel Algorithms for Short-Range Molecular Dynamics, J. Comput. Phys. 117 (1995) 1–19, https://doi.org/10.1006/jcph.1995.1039.
[48] LAMMPS pair-style reax. Sandia National Laboratories. http://lammps.sandia.gov/doc/pair_reax.html, (s. f.).
[49] O. García-Beltrán, B.K. Cassels, N. Mena, M.T. Nuñez, O. Yañez, J. Caballero, A coumarinylaldoxime as a specific sensor for Cu2+ and its biological application, Tetrahedron Lett. 55 (2014) 873–876, https://doi.org/10.1016/j.tetlet.2013.12.033.
[50] L.F. Zhang, J.L. Zhao, X. Zeng, L. Mu, X.K. Jiang, M. Deng, J.X. Zhang, G. Wei, Tuning with pH: The selectivity of a new rhodamine B derivative chemosensor for Fe3+ and Cu2+, Sensors Actuators, B Chem. 160 (2011) 662–669, https://doi.org/10.1016/j.snb.2011.08.045.
[51] Y. Hu, J. Zhang, Y.Z. Lv, X.H. Huang, S.L. Hu, A new rhodamine-based colorimetric chemosensor for naked-eye detection of Cu 2 + in aqueous solution, Spectrochim. Acta - Part A Mol. Biomol. Spectrosc. 157 (2016) 164–169, https://doi.org/10.1016/j.saa.2015.12.031.
[52] S. Goswami, D. Sen, A.K. Das, N.K. Das, K. Aich, H.K. Fun, C.K. Quah, A.K. Maity, P. Saha, A new rhodamine-coumarin Cu2+-selective colorimetric and "off-on" fluorescence probe for effective use in chemistry and bioimaging along with its bound X-ray crystal structure, Sensors Actuators, B Chem. 183 (2013) 518–525, https://doi.org/10.1016/j.snb.2013.04.005.
[53] P.W. Cheah, M.P. Heng, H.M. Saad, K.S. Sim, K.W. Tan, Specific detection of Cu2+ by a pH-independent colorimetric rhodamine based chemosensor, Opt. Mater. (Amst). 114 (2021), 110990, https://doi.org/10.1016/j.optmat.2021.110990.
[54] Y. Hu, J. Zhang, Y. Lv, X. Huang, S. Hu, Spectrochimica Acta Part A : Molecular and Biomolecular Spectroscopy A new rhodamine-based colorimetric chemosensor for naked-eye detection of Cu 2 + in aqueous solution, 157 (2016) 164–169.
[55] B. Zhang, Q. Diao, P. Ma, X. Liu, D. Song, X. Wang, Sensors and Actuators B : Chemical A sensitive fluorescent probe for Cu 2 + based on rhodamine B derivatives and its application to drinking water examination and living cells imaging, 225 (2016) 579–585.
[56] E. Wang, Y. Zhou, Q. Huang, L. Pang, H. Qiao, F. Yu, B. Gao, J. Zhang, Spectrochimica Acta Part A : Molecular and Biomolecular Spectroscopy 5-Hydroxymethylfurfural modified rhodamine B dual-function derivative : Highly sensitive and selective optical detection of pH, 152 (2016) 327–335.
[57] W.N. Wu, H. Wu, R. Bin Zhong, Y. Wang, Z.H. Xu, X.L. Zhao, Z.Q. Xu, Y.C. Fan, Ratiometric fluorescent probe based on pyrrole-modified rhodamine 6G hydrazone for the imaging of Cu 2+ in lysosomes, Spectrochim. Acta - Part A Mol. Biomol. Spectrosc. 212 (2019) 121–127. 10.1016/j.saa.2018.12.041.
[58] M. Tian, H. He, B. Wang, X. Wang, Y. Liu, F. Jiang, Dyes and Pigments A reaction-based turn-on fl uorescent sensor for the detection of Cu (II) with excellent sensitivity and selectivity : Synthesis, DFT calculations, kinetics and application in real water samples, Dye. Pigment. 165 (2019) 383–390, https://doi.org/10.1016/j.dyepig.2019.02.043.
[59] F.N. Arslan, G.A. Geyik, K. Koran, F. Ozen, D. Aydin, Ş. Nihan, K. Elmas, Fluorescence " Turn On – Off " Sensing of Copper (II) Ions Utilizing Coumarin – Based Chemosensor : Experimental Study, Mineral and Drinking Water Analysis, Theoretical Calculation, 2020, pp. 317–327.
[60] G. Kim, D. Choi, C. Kim, A Benzothiazole-Based Fluorescence Turn-on Sensor for Copper (II), (2021) 1203–1209.
[61] G.T. Selvan, C. Varadaraju, R.T. Selvan, I.V.M. V Enoch, P.M. Selvakumar, On / O ff Fluorescent Chemosensor for Selective Detection of Divalent Iron and Copper Ions : Molecular Logic Operation and Protein Binding, (2018). 10.1021/acsomega.8b00748.
[62] L. Qu, C. Yin, F. Huo, J. Chao, Y. Zhang, Sensors and Actuators B : Chemical A pyridoxal-based dual chemosensor for visual detection of copper ion and ratiometric fluorescent detection of zinc ion, Sensors Actuators B. Chem. 191 (2014) 158–164, https://doi.org/10.1016/j.snb.2013.09.114.
[63] M. Aarjane, S. Slassi, A. Amine, Novel highly selective and sensitive fl uorescent sensor for copper detection based on N -acylhydrazone acridone derivative, J. Mol. Struct. 1199 (2020), 126990, https://doi.org/10.1016/j.molstruc.2019.126990.
[64] B. Wang, W. Xu, K. Gan, K. Xu, Q. Chen, W. Wei, W. Wu, Spectrochimica Acta Part A : Molecular and Biomolecular Spectroscopy On the synthesis and performance of a simple colorimetric and fluorescent chemosensor for Cu 2 + with good reversibility, 277 (2022) 1–7. 10.1016/j.saa.2022.121245.
[65] A.K. Kudva, S.V. Raghu, Short communication A versatile rhodamine B-derived fluorescent probe for selective copper (II) sensing, Inorg. Chem. Commun. 141 (2022), 109501, https://doi.org/10.1016/j.inoche.2022.109501.
[66] S. Sawminathan, S. Munusamy, S. Manickam, A simple quinazolinone-isophorone based colorimetric chemosensor for the reversible detection of copper (II) and its application in real samples, J. Mol. Struct. 1257 (2022), 132633, https://doi.org/10.1016/j.molstruc.2022.132633.
[67] J.A.E.S. Heo, B. Suh, C. Kim, Selective detection of Cu 2 + by benzothiazole-based colorimetric chemosensor : a DFT study, J. Chem. Sci. (2022) 1–10, https://doi.org/10.1007/s12039-022-02037-1.
[68] A.N. Meshkov, G.A. Gamov, Talanta KEV : A free software for calculating the equilibrium composition and determining the equilibrium constants using UV – Vis and potentiometric data, Talanta. 198 (2019) 200–205, https://doi.org/10.1016/j.talanta.2019.01.107.
[69] G.A. Gamov, A.N. Meshkov, M.N. Zavalishin, M.V. Petrova, A.Y. Khokhlova, A. V. Gashnikova, V.A. Sharnin, Spectrochimica Acta Part A : Molecular and Biomolecular Spectroscopy Binding of pyridoxal, pyridoxal 5 ′ -phosphate and derived hydrazones to bovine serum albumin in aqueous solution, Spectrochim, Acta Part A Mol. Biomol. Spectrosc. 233 (2020), 118165, https://doi.org/10.1016/j.saa.2020.118165.
[70] G.A. Zhurko, D.A. Zhurko, Chemcraft - graphical software for visualization of quantum chemistry computations., (2018).